Identification of a Kinase-Active CheA Conformation in *Escherichia coli* Chemoreceptor Signaling Complexes

Germán E. Piñas,[a] John S. Parkinson[a]

[a]School of Biological Sciences, University of Utah, Salt Lake City, Utah, USA

ABSTRACT *Escherichia coli* chemotaxis relies on control of the autophosphorylation activity of the histidine kinase CheA by transmembrane chemoreceptors. Core signaling units contain two receptor trimers of dimers, one CheA homodimer, and two monomeric CheW proteins that couple CheA activity to receptor control. Core signaling units appear to operate as two-state devices, with distinct kinase-on and kinase-off CheA output states whose structural nature is poorly understood. A recent all-atom molecular dynamic simulation of a receptor core unit revealed two alternative conformations, "dipped" and "undipped," for the ATP-binding CheA.P4 domain that could be related to kinase activity states. To explore possible signaling roles for the dipped CheA.P4 conformation, we created CheA mutants with amino acid replacements at residues (R265, E368, and D372) implicated in promoting the dipped conformation and examined their signaling consequences with *in vivo* Förster resonance energy transfer (FRET)-based kinase assays. We used cysteine-directed *in vivo* cross-linking reporters for the dipped and undipped conformations to assess mutant proteins for these distinct CheA.P4 domain configurations. Phenotypic suppression analyses revealed functional interactions among the conformation-controlling residues. We found that structural interactions between R265, located at the N terminus of the CheA.P3 dimerization domain, and E368/D372 in the CheA.P4 domain played a critical role in stabilizing the dipped conformation and in producing kinase-on output. Charge reversal replacements at any of these residues abrogated the dipped cross-linking signal, CheA kinase activity, and chemotactic ability. We conclude that the dipped conformation of the CheA.P4 domain is critical to the kinase-active state in core signaling units.

IMPORTANCE Regulation of CheA kinase in chemoreceptor arrays is critical for *Escherichia coli* chemotaxis. However, to date, little is known about the CheA conformations that lead to the kinase-on or kinase-off states. Here, we explore the signaling roles of a distinct conformation of the ATP-binding CheA.P4 domain identified by all-atom molecular dynamics simulation. Amino acid replacements at residues predicted to stabilize the so-called "dipped" CheA.P4 conformation abolished the kinase activity of CheA and its ability to support chemotaxis. Our findings indicate that the dipped conformation of the CheA.P4 domain is critical for reaching the kinase-active state in chemoreceptor signaling arrays.

KEYWORDS chemotaxis, molecular dynamics, *in vivo* FRET, CheA kinase

*E*scherichia coli and many other motile bacteria monitor and track chemical gradients to reach favorable living environments, a behavior known as chemotaxis. The *E. coli* chemosensing apparatus comprises membrane-bound chemoreceptors, a small adaptor protein (CheW), and the cytoplasmic histidine kinase CheA, which plays a central role in the signal transduction pathway. Using ATP as a phosphodonor, CheA autophosphorylates at a histidine residue (1). Phospho-CheA in turn serves as a phosphodonor for the CheY response regulator, which is phosphorylated at an aspartate residue
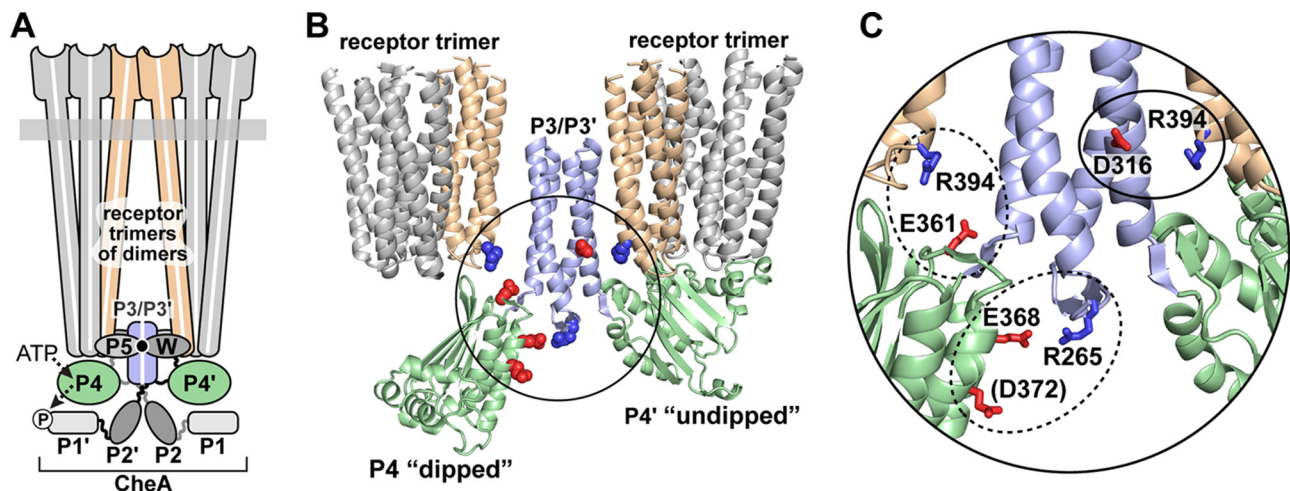
FIG 1 Configurations of the CheA.P4 domain in the receptor core complex. (A) Schematic representation of a core signaling complex (side view). Periplasmic sensing domains of the receptor dimers lie at the top of the figure; the gray rectangle represents the cytoplasmic membrane. The cytoplasmic tips of the receptors interact to form trimers of dimers. One receptor in each trimer (tan) binds a CheW molecule (W). Each CheW in turn binds to a CheA.P5 domain at their interface 1 surfaces (black circle) to construct the signaling complex. CheA has five domains in each subunit: P1 (phosphorylation site), P2 (CheB and CheY binding), P3 (dimerization), P4 (ATP binding), and P5 (CheW and receptor interaction). Note that CheA autophosphorylation is a *trans* reaction, involving interaction of a P1 domain in one subunit with a P4 domain in the other. White lines in the receptors and in the P3/P3′ domains of CheA indicate the dimerization interface between the two protomers of the homodimers. (B) "Dipped" and "undipped" conformations of the CheA.P4 domain. This structural model comes from an all-atom molecular dynamics simulation of a *Thermotoga maritima* core complex (25). Basic (blue) and acidic (red) residues in salt bridges that distinguish the two conformations are indicated. The coloring scheme approximates that in panel A. (C) Detailed view of salt bridge pairs in the two CheA.P4 conformations. Although the structure depicts the *T. maritima* complex, the residue numbers indicate the *E. coli* Tsr and CheA proteins investigated in the present study. Tsr-R394/CheA-D316 (solid circle) characterize the undipped conformation. Tsr-R394/CheA-E361 and CheA-R265/-E368 (dashed circles) characterize the dipped conformation. Another probable R265 interaction partner (D372), not reported by Cassidy et al. (25), was discovered in the present study.

(2). Phospho-CheY (P-CheY) engages the basal bodies of the cell's flagellar motors to promote clockwise rotation, which produces random changes ("tumbles") in swimming direction (3). P-CheY turns over rapidly in the cell through the action of a dedicated phosphatase, CheZ (4). At low P-CheY levels, the flagellar motors adopt their default counterclockwise rotation mode, which produces smooth forward-swimming movements. When the cell swims in a chemoeffector gradient, its receptor signaling complex responds to increasing attractant concentrations by downregulating CheA autophosphorylation activity. The resulting reduction in P-CheY level promotes forward swimming and up-gradient travel (5).

Chemoreceptor core complexes, the minimal signaling unit, comprise two trimers of receptor homodimers, which can contain receptors of different detection specificities, two monomeric CheW molecules, and one homodimeric CheA molecule (6). CheA subunits contain five domains: P1 (phosphorylation site), P2 (CheB and CheY binding), P3 (dimerization), P4 (ATP binding), and P5 (CheW binding) (Fig. 1A). The CheW molecules couple CheA to receptor control through two different binding interactions, one with a receptor dimer in each trimer and another, at designated interface 1, with the CheA.P5 domain (Fig. 1A). A second CheA.P5·CheW interaction, at designated interface 2 (not shown), connects core units into highly cooperative, hexagonally packed arrays (7–9).

During CheA autophosphorylation, the P4 domain of one subunit interacts with the P1 domain of the other subunit to promote a *trans* reaction (10, 11) CheA alone autophosphorylates at a slow basal rate, but its activity increases dramatically in core signaling units: ligand-free receptors enhance CheA autophosphorylation several hundredfold. In contrast, attractant-bound receptors inhibit CheA activity to basal levels (12, 13). Core complexes are able to activate/deactivate CheA as effectively as receptor arrays, indicating that the molecular events leading to receptor control of CheA activity occur at the core unit level (6, 9, 14). Receptor complexes probably stimulate CheA activity above basal level by enhancing the frequency of productive P1-P4′ encounters

(15, 16). The interdomain linkers (L) flanking P4 (L3 joins P3 to P4; L4 joins P4 to P5) also appear to play critical roles in CheA activation and receptor control (17–19).

Although the P4 and P1 residues involved in ATP binding and phosphorylation are well defined (1, 20), and contact points between these domains have been identified (16, 21–23), the molecular mechanism(s) of CheA control in receptor signaling units is still poorly understood. Enzymatic analyses indicated that kinase control in core complexes occurs mainly through modulation of the reaction rate (k_{cat}) rather than the interaction affinity between the P1 and P4 domains (14). Nevertheless, several lines of evidence suggest that changes in domain positioning are important in CheA control (15, 16, 19, 24).

Cryo-electron microscopy (cryo-EM) and molecular dynamics (MD) studies have identified CheA conformations in the core signaling unit that could be relevant to the receptor control mechanism(s), namely, an "undipped" state, in which P4 lies close to the receptor tip and the CheA.P5 domain, and a "dipped" state, in which P4 extends away from the receptor tip (25; C. K. Cassidy, B. A. Himes, D. Sun, J. Ma, G. Zhao, J. S. Parkinson, P. J. Stansfeld, Z. Luthey-Schulten, and P. Zhang, submitted for publication) (Fig. 1B). The dipped and undipped structures exhibited differences in salt bridge residue pairs that might stabilize the alternative conformations. Our study explores the functional roles of CheA residues R265, E368, and D372 that may specifically stabilize the dipped P4 conformation (25) (Fig. 1C). We also explored two alternative interactions between a conserved arginine residue in the chemoreceptor tip (Tsr-R394) and CheA acidic residues (E361 and D316) that distinguish the dipped and undipped states, respectively (25) (Fig. 1C). We characterized the signaling properties of receptor and CheA mutants with a variety of amino acid replacements at each of these residues and found that the dipped CheA conformation plays an essential role in the CheA reaction cycle.

RESULTS

To investigate the signaling roles of salt bridge pairs associated with the dipped or undipped P4 conformations, we created mutant CheA and receptor proteins with various amino acid replacements (A, G, L, T, K and/or R, D and/or E, and N and/or Q) at each of the residues shown in Fig. 1C. We first measured the steady-state levels of the mutant proteins to ensure that any defects they exhibited in function tests were not caused by reduced expression or stability. All mutant proteins had intracellular levels within the wild-type range (see Tables S1 and S3 in the supplemental material). We then characterized their signaling properties with semisolid agar chemotaxis assays and a Förster resonance energy transfer (FRET)-based *in vivo* kinase assay (26, 27). The FRET assay measures receptor-coupled CheA activity in a population of about 500 cells and the activity changes elicited by attractant stimuli. We fit the dose-response behaviors to a multisite Hill equation to obtain values for the response $K_{1/2}$ (the concentration of attractant that inhibits 50% of the kinase activity, a measure of detection sensitivity), the Hill coefficient (a measure of response cooperativity), and overall kinase activity in the mutant core complexes (see Materials and Methods).

CheA residues R265, E368, and D372. The side chains of CheA residues E368 and R265 interact in the dipped conformation (25). D372 is one helical turn away from E368 and could conceivably also interact with R265, so we tested that position as well (Fig. 1C). We created mutant derivatives at these three residues in plasmid pPM25, which expresses the CheA and CheW proteins under salicylate-inducible control (9) We assessed their ability to support chemotaxis in strain UU2683, which lacks the chromosomal *cheA* and *cheW* genes and receptor genes *tar*, *tap*, *trg*, and *aer* (9). UU2683 expresses Tsr, the serine sensor, as its only chemoreceptor. When complemented with wild-type pPM25, UU2683 exhibits robust serine chemotaxis (Fig. 2C). The kinase activities and serine control responses of mutant pPM25 derivatives were measured in strain UU2784 containing a compatible plasmid (pVS88) that expresses the FRET reporter proteins CheY-yellow fluorescent protein (YFP) and CheZ-cyan fluorescent protein (CFP) under isopropyl-β-D-thiogalactopyranoside (IPTG)-inducible control (27).
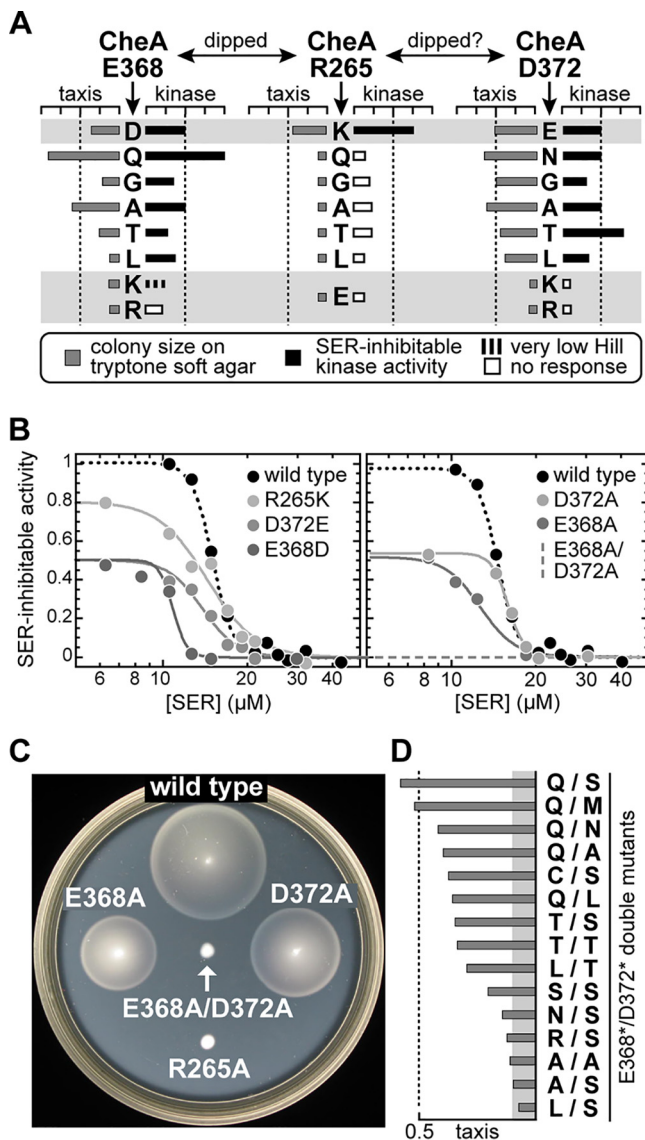
FIG 2 Functional properties of CheA-R265, CheA-E368, and CheA-D372 mutants. Plasmid pPM25 derivatives were assessed in strain UU2683 for the ability to support chemotaxis in tryptone soft agar assays and in strain UU2784 to determine kinase activities and serine control responses by *in vivo* FRET assays (see Materials and Methods). (A) Chemotaxis and *in vivo* kinase activities of R265, E368, and D372 mutants. Amino acid replacements are denoted by single-letter designations below the wild-type residue. Histogram bars indicate chemotaxis (gray) and serine-inhibitable kinase activities for each mutant protein, normalized to the corresponding wild-type values. Dashed lines denote 0.5 of the wild-type performance. Broken black bars indicate low-cooperativity serine responses (Hill < 3); white bars indicate little or no kinase activity and no response to a saturating serine stimulus. (B) Serine dose-response curves from FRET kinase assays of representative CheA mutants in strain UU2784, which lacks the CheR and CheB sensory adaptation enzymes. Parameter values for all mutants are provided in Table S1. (C) Chemotaxis performance of CheA mutants with single or double alanine replacements. Mutant plasmid derivatives were tested in strain UU2683, which is adaptation competent and expresses wild-type Tsr as its only receptor. The tryptone soft agar plate was incubated at 32.5°C for 7 h. (D) Chemotaxis promoted by E368*/D372* doubly mutant proteins in strain UU2683. Taxis values are colony sizes on tryptone soft agar, normalized to that of the wild-type control. Values that fall within the gray rectangle are comparable to those of the empty vector control. See Table S2 for data values. Asterisks indicate amino acid replacements at position E368 or D372.

UU2784 lacks the chromosomal *cheA*, *cheW*, *cheY*, and *cheZ* genes and expresses Tsr as its only chemoreceptor (9). Unlike UU2683, UU2784 also lacks the *cheR* and *cheB* genes that encode the sensory adaptation enzymes, thus ensuring a homogeneous QEQEE residue pattern at the modification sites in each Tsr subunit and no adaptational

recovery following the response to a serine stimulus. In the adaptation-deficient UU2784 host, the parental pPM25 plasmid produced a $K_{1/2}$ response to serine of 17 ± 1 μM, with high cooperativity (Hill coefficient = 18 ± 3).

The chemotaxis abilities and kinase activities of the mutants are summarized in Fig. 2A (see also Table S1). Consistent with the Cassidy et al. report (25), CheA-R265 proved to be a functionally critical residue. All but one R265 amino acid replacement abrogated both chemotaxis in the soft agar assay and serine responses in the FRET assay. The mutant R265 proteins produced low kinase activity, most of them less than 25% of the wild-type level (Fig. 2A; Table S1). The like-charge R265K protein supported about 50% chemotaxis performance and more than 50% of the wild-type kinase activity, but responded to serine stimuli with much reduced cooperativity (Fig. 2B; Table S1). These results demonstrate that residue R265 of CheA promotes kinase activity and stimulus control in receptor signaling complexes.

The E368A and E368Q mutants retained substantial chemotactic ability and kinase activity, but other replacements at this position (D, G, L, K, T, or R) reduced both chemotaxis performance and kinase activity to less than 50% of wild-type levels (Fig. 2A). All E368 mutants except E368R downregulated their kinase activity after a serine stimulus, but most of them (A, G, K, L, or T) responded with moderately reduced cooperativity (Fig. 2B; Table S1). These results suggest that E368 has an important role in kinase activity and control, but the considerable functionality of the E368A protein indicates that E368 is not as critical as its putative interaction partner, R265.

Most D372 amino acid replacement mutants (A, E, G, N, or T) retained nearly 50% or more of wild-type chemotaxis ability and 25 to 50% of wild-type kinase activity (Fig. 2A). These mutants also responded to serine stimuli with nearly normal sensitivity and with much of the wild-type cooperativity (Fig. 2A; D372A and D372E in Fig. 2B; Table S1). These results indicate that the side chain character at CheA residue 372 is not critical for proper kinase activity and control. However, the charge reversal mutants, D372K and D372R, were fully defective in these functions. Conceivably, their more drastic functional defects arise from charge-repulsion interactions with R265 or charge-attraction interactions with E368.

An alanine replacement at either E368 or D372 had only modest effects on signaling function, consistent with the possibility that these two residues play redundant roles in an interaction with R265. To test this idea, we constructed and characterized a doubly mutant protein with A replacements at both residues. The E368A/D372A mutant produced no kinase activity and could not support chemotactic behavior (Fig. 2B and C). Based on the single-mutant phenotypes, we conclude that E368 is the more functionally important interaction partner for R265 but that the D372 residue may assume this role in some E368 mutants, including E368A. Consistent with this supposition, we found that a majority of other E368/D372 double mutants displayed 30 to 50% of wild-type chemotaxis if either position carried a polar replacement (Fig. 2D). This observation suggests that polar interactions between the native R265 and positions 368 and 372 can sustain some CheA function.

To probe possible structural and functional interactions between R265 and its putative partners, we searched for amino acid replacements at E368 and/or D372 that could suppress the chemotaxis defect of an R265 mutant. Accordingly, we performed all-codon mutagenesis at *cheA* codons 368 and 372 in R265 mutant plasmids and looked for derivatives that restored chemotaxis in strain UU2683. We failed to obtain suppressors of R265E or R265L but succeeded with R265T and R265Q, which presumably have less drastic structural alterations. In each case, the targeted E368 and D372 residues yielded a different set of suppressors, some of which were independently obtained multiple times. Thus, it seems unlikely that any other amino acid replacements at E368 or D372 can suppress R265T or R265Q to a similar extent. We obtained single E368 or D372 suppressors, all with polar side chain replacements (Fig. 3A; Table S1). We also found doubly mutant suppressors that had at least one polar replacement at either E368 or D372; side chain character at the second residue had little effect on suppression efficiency (Fig. 3A; Table S2). In FRET assays, the R265T|Q suppressors
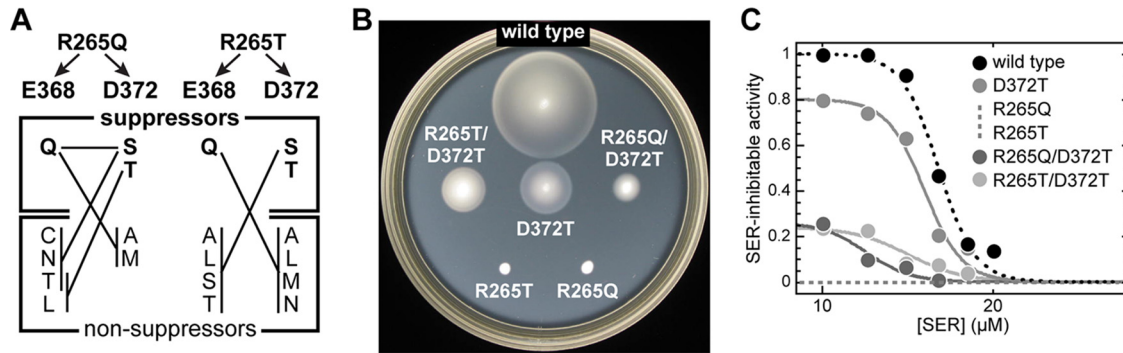
FIG 3 Phenotypic suppression of CheA-R265 mutants. (A) Replacements at CheA residues E368 and D372 that restored chemotaxis to CheA-R265Q and CheA-R265T mutants. Suppressors were isolated from strain UU2683 transformed with mutagenized pPM25 derivatives. Amino acid changes that suppressed R265Q or R265T are indicated in bold letters, listed vertically from most to least effective, below the targeted residues (E368 or D372). Lines connecting residue changes at E368 and D372 identify double mutant combinations that retained suppression activity. The criterion for suppression was a colony size on tryptone soft agar at least 20% of the wild-type control size. All parameter values are given in Table S2. (B) Two examples of suppression effects. Mutant plasmids were assessed in strain UU2683 on tryptone soft agar plates incubated at 32.5°C for 7 h. (C) Serine response behaviors of the CheA mutants shown in panel B. Kinase activities and serine responses were determined by *in vivo* FRET assays in strain UU2784.

restored up to ~40% of wild-type kinase activity and nearly wild-type serine response thresholds. The signaling properties of the single suppressor CheA proteins are summarized in Table S1; the functional effects of a representative suppressor (D372T) are shown in Fig. 3B and C.

CheA R265, E368, and D372 act independently of the P2-P3 linker. Residue R265 is located at the N terminus of the P3 domain (see Fig. 1C); it might promote catalytic P1-P4′ interactions by directing the P2-P3 linker toward the *trans* subunit of the CheA dimer (16, 24, 25). Such a mechanistic role predicts that side chain replacements at R265 or at its interacting partners (E368 and D372) could reduce CheA activity by impairing the *trans* positioning of the P2-P3 linker. To test this hypothesis, we evaluated the ability of CheA.P3-P4-P5 fragments bearing a charge reversal replacement at R265, E368, or D372 to phosphorylate free P1 fragments. *In vivo*, the P3-P4-P5 portion of CheA efficiently phosphorylates free P1 domains expressed in excess (28) and thereby supports chemotaxis in the absence of the CheA.P2 domain, which is not essential for phosphotransfer to CheY or CheB (29, 30) (Fig. 4A and B). It follows that CheA alterations that simply affect positioning of the P2-P3 linker in full-length CheA should not prevent phosphorylation of free P1 domains. However, when tested in tryptone soft
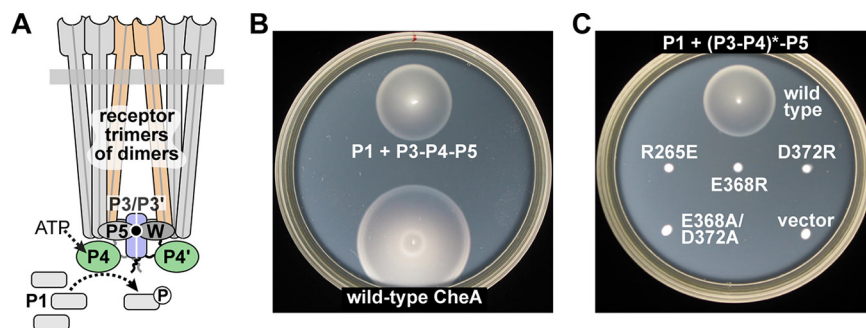

FIG 4 Chemotactic ability of cells expressing free CheA.P1 fragments in combination with CheA.P3.P4.P5 fragments. (A) Schematic of the function test. Domain cartoons and colors follow the conventions in Fig. 1A. In appropriate excess, free CheA.P1 domains can obtain sufficient phosphoryl groups from CheA.P3.P4.P5 fragments in receptor signaling complexes to support chemotaxis (28). (B) Chemotaxis supported by CheA.P3.P4.P5 fragments compared to that of wild-type CheA. Chemotaxis was assessed on tryptone soft agar plates in strain UU2683 [Δ(cheAW)] cotransformed with plasmid pPM25 (CheA/CheW) and pCJ30 (empty vector) or with plasmid pGP67 (CheA.P3.P4.P5 CheW) and pAG17 (CheA.P1). (C) Chemotaxis supported by CheA.P1 and mutant CheA.P3.P4.P5 fragments. Chemotaxis was assessed as in panel B, but with pGP67 derivatives bearing replacements at the indicated CheA residues.

agar plates, none of the charge reversal mutants or the E368A/D372A double mutant supported colony expansion in the bipartite function test (Fig. 4C), implying that their structural changes affect critical molecular events in the catalytic CheA core (P3-P4) independent of the presence, position, or conformation of the P2-P3 linker.

Core complex and array assembly by the R265E, E368R, and D372R proteins. A charge reversal replacement at any member of the putative salt bridge team (R265-E368 and D372) produced the most drastic loss of kinase activity and control in core signaling complexes, implying that such lesions disrupt CheA structural features needed to reach a kinase-active conformation or dynamic state. To determine whether the charge reversal proteins are able to assemble signaling clusters, we prepared mutant derivatives of plasmid pAV232, which encodes CheW and a CheA protein in which monomeric YFP (mYFP) replaces the P2 domain (9). The pAV232 charge reversal derivatives (R265E, E368R, and D372R) were examined by fluorescence light microscopy for cluster formation in strain UU2806 (chromosomal deletions of *cheA*, *cheW*, and all receptor genes), which also carried plasmid pRR53 to supply the wild-type Tsr receptor (see Materials and Methods). All CheA charge reversal proteins showed clustering patterns and efficiencies comparable to those of the wild-type control protein (Fig. S1). We conclude that these CheA lesions do not impair core complex assembly or receptor cluster formation.

We also probed the ability of the CheA charge reversal proteins to interact with CheW at array interface 2, an interaction that assembles core signaling complexes into cooperative arrays (9). We constructed charge reversal mutants of plasmid pGP55, a derivative of pPM25 that expresses interface 2 cross-linking reporters CheA-A546C and CheW-E27C (9). Known interface 2 lesions substantially reduce disulfide cross-linking between these reporter proteins (9), but the CheA charge reversal changes did not (Fig. S2A). We conclude that the charge reversal proteins mediate unimpaired interface 2 interactions.

We used a related cross-linking assay to probe the ability of the charge reversal CheA proteins to interact with CheW at array interface 1, which is critical for assembly and operation of core signaling units (31). Accordingly, we created charge reversal mutants of plasmid pGP58, a derivative of pPM25 that expresses interface 1 cross-linking reporters CheA-S630C and CheW-Q44C (31). In our hands, interface 1 interactions proved relatively robust *in vivo*. A single interface 1 lesion in either CheA or CheW had little effect on cross-link formation, whereas lesions in both partners eliminated the cross-linking signal (Fig. S2B, lower panel). In this assay, none of the charge reversal lesions impacted the CheA-CheW interface 1 interaction (Fig. S2B, upper panel).

Overall, these clustering and cross-linking tests indicate that the CheA charge reversal proteins (R265E, E368R, and D372R) assemble core signaling units and efficiently link them into receptor arrays.

Basal autophosphorylation activities of the R265E, E368R, and D372R proteins. We purified 8×His–Twin-Strep (HTS)-tagged CheA charge reversal proteins and measured their autophosphorylation activity *in vitro* (see Materials and Methods). The R265E protein showed roughly half of wild-type CheA basal activity, whereas it was relatively much less active in receptor-coupled signaling complexes *in vivo* (Fig. 5A). In contrast, the E368R and D372R proteins outperformed wild-type CheA by roughly 2- to 4-fold in basal autophosphorylation rate (Fig. 5A). These results show that a charge reversal replacement at R265 impacts both basal and coupled CheA activity, whereas a charge reversal at either of its acidic residue partners (E368 and D372) impairs only the receptor-coupled activity (Fig. 5A).

Structural consequences of charge reversals at R265, E368, and D372. In their MD study, Cassidy et al. (25) reported cross-linking assays for the alternative P4 conformations that used Tsr-R394C paired with CheA-E361C (dipped state) or CheA-D316C (undipped state) (Fig. 1C). We employed the same reporter sites to probe the effects of R265, E368, and D372 charge reversals on the dipped and undipped cross-linking signals. We created mutant derivatives of plasmids pGP57-CheA-E361C and
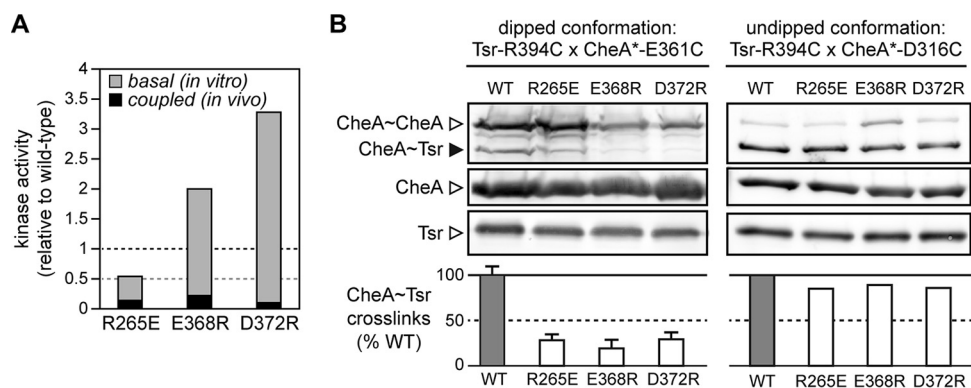
FIG 5 Basal kinase activities and cross-linking properties of CheA charge reversal mutants. (A) Kinase activities of CheA mutants. Receptor-coupled data come from *in vivo* FRET assays of mutant pPM25 derivatives in strain UU2784 treated with 3 mM KCN (see Table S1). Basal CheA activities were measured *in vitro* with purified CheA proteins, using a coupled enzymatic assay to follow ATP hydrolysis (19). (B) Cross-linking assays for the dipped and undipped P4 conformations. Tsr-R394C/CheA-E361C and Tsr-R394C/CheA-D316C were used as cross-linking reporters (25). Cross-linking was induced by bismaleimidoethane (BMOE) treatment of UU2960 cells expressing the reporter proteins from plasmids pRR53-R394C and pGP57-E361C or pGP57-D316C derivatives that also carried CheA charge reversal changes. Lysate proteins were separated by SDS-PAGE and probed with antihemagglutinin (anti-HA) antibody (Pierce) to detect CheA and CheA≈Tsr cross-linking products. Tsr expression was determined with a polyclonal anti-Tsr antibody. Histogram bars indicate the fraction of CheA subunits cross-linked to Tsr; error bars indicate the standard error of three measurements.

pGP57-CheA-D316C, which respectively encode hemagglutinin (HA)-tagged CheA proteins with the E361C and D316C reporters, and paired those plasmids with a pRR53 derivative encoding Tsr-R394C in strain UU2960. This strain lacks all chemoreceptors and CheA, CheW, CheR, and CheB proteins, but expresses CheY and CheZ to allow for phosphate flux from plasmid-encoded CheA variants. All three charge reversal lesions reduced cross-linking of the dipped conformation reporters to about 25% or less than that of the wild-type control (Fig. 5B). In contrast, those lesions had little impact on cross-linking of the undipped conformation reporters, producing at least 85% of the wild-type control value (Fig. 5B). These results indicate that the CheA structural features affected by the R265, E368, and D372 charge reversal replacements are uniquely deleterious to the dipped P4 conformational state.

CheA-D316, Tsr-R394, and CheA-E361. We created mutant derivatives of CheA residues 316 and 361 in plasmid pPM25 and characterized them with functional assays in the UU2683 and UU2784 hosts, as described above. We created mutant Tsr-R394 derivatives by all-codon mutagenesis of plasmid pRR53, which expresses the *tsr* gene under IPTG-inducible control (32). The corresponding hosts for Tsr functional assays were UU2612—which lacks all receptor genes but has wild-type genes for CheA and CheW and for the sensory adaptation enzymes CheR and CheB—and UU2567, a receptorless FRET host that has wild-type genes for CheA and CheW but lacks the sensory adaption enzymes (33). The chemotaxis abilities and kinase activities of these Tsr and CheA mutants are summarized in Fig. 6A (see also Table S3).

All but one CheA-D316 mutant exhibited essentially wild-type function (Fig. 6A). The lone exception, D316R, produced a normal level of kinase activity but supported less than 50% of wild-type chemotaxis, possibly due to the low cooperativity of its serine control response (Table S3). These results indicate that side chain character at CheA residue D316 is not critical for kinase activity or control in receptor signaling complexes.

Amino acid replacements at CheA residue E361, including charge reversals, also allowed considerable functionality. Although most of the mutant proteins supported less than 50% of wild-type chemotaxis ability, all exhibited 50% or more of the wild-type kinase activity and responded to serine control with high cooperativity (Fig. 6A; Table S3). The E361R mutant was the only one to exhibit reduced response cooperativity (Fig. 6B; Table S3). Clearly, side chain character at CheA residue E361 is also not critical for kinase activity or control.
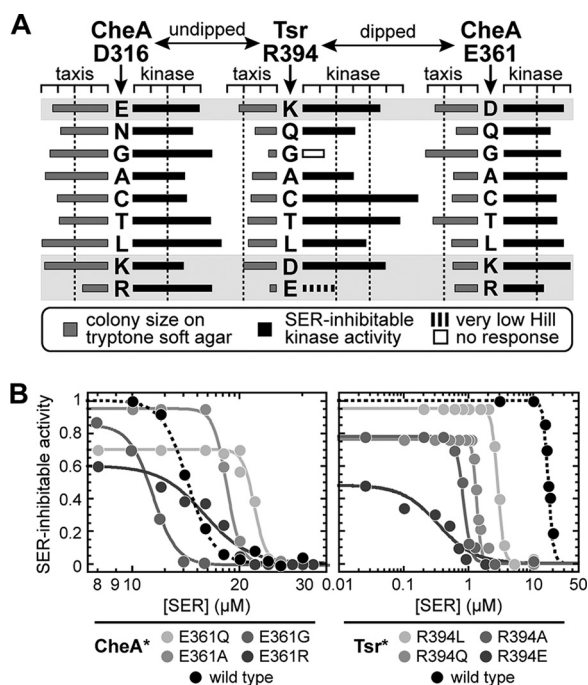
FIG 6 Functional properties of CheA-D316, CheA-E361, and Tsr-R394 mutants. Chemotaxis and serine responses of CheA mutants were assessed in strains UU2683 and UU2784 bearing pPM25 derivatives. Derivatives of pPA114 expressing Tsr-R394 mutants were tested for chemotaxis in strain UU2612 and for serine responses in strain UU2567. (A) Chemotaxis and *in vivo* kinase activities. Histogram bars indicate chemotaxis and serine-inhibitable kinase activities, normalized to the corresponding wild-type values. Dashed lines denote 0.5 increments of the wild-type performance. Broken black bars indicate low-cooperativity serine responses (Hill < 3); white bars indicate little or no kinase activity and no response to a saturating serine stimulus. (B) Serine dose-response curves of representative CheA mutants in strain UU2784 (left) and of representative Tsr-R394 mutants in strain UU2567 (right). Both of the FRET tester strains lack the CheR and CheB sensory adaptation enzymes. Parameter values for all mutants are provided in Table S3.

All amino acid replacements at Tsr-R394 impaired chemotaxis performance to various extents (Fig. 6A; Table S3). The like-charge R394K mutant was most functional, but mutants with either polar or nonpolar replacements (A, D, K, L, Q, or T) also exhibited near-normal kinase activities and serine response cooperativities (Fig. 6; Table S3). The charge reversal R394E mutant also produced ample kinase activity but responded to serine with very low cooperativity (Fig. 6B; Table S3). Except for R394K, all of the serine-responsive mutants had significantly enhanced detection sensitivities (Table S3); Fig. 6B shows examples of their dose-response curves. In contrast, the R394G protein was fully defective in both chemotaxis and kinase activity. Based on these results, we conclude that Tsr-R394 is important to chemotaxis performance but does not play a critical role in generating or regulating kinase activity in receptor signaling complexes.

DISCUSSION

Structural basis of receptor-activated CheA autophosphorylation. The autophosphorylation rate of the CheA protein alone is less than 1% of that in kinase-active receptor signaling complexes (6, 12–14). Optimized cryo-electron tomography (cryo-ET) and MD models of the ternary signaling complex require rotation of the CheA.P5 domains relative to their orientations in the CheA.P3-P4-P5 crystal structure (7, 8, 19, 24, 25, 34). The CheA homodimer in solution is quite dynamic, and its various domains move extensively relative to one another (16, 19, 21). Thus, CheA basal activity probably requires a domain arrangement(s), seldom achieved in solution, that approximates those in core complexes. Stabilization of CheA interdomain interfaces may be largely responsible for the high rate of autophosphorylation activity in core complexes.
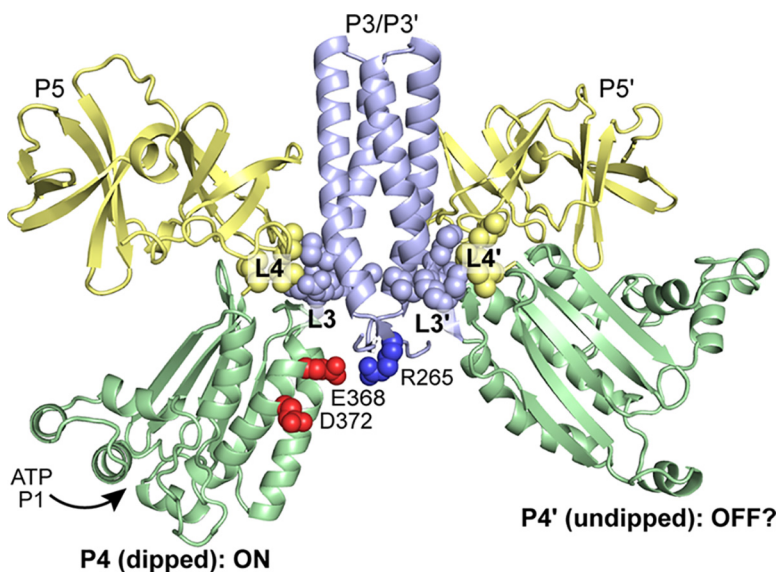
FIG 7 CheA structural features important for activity and control in receptor signaling complexes. This image was prepared from the *T. maritima* atomic coordinates that are also used in Fig. 1 (25). The receptor and CheW components of the core complex are omitted; side chain atoms of the linker residues flanking the P4 domain are space filled (L3, blue; L4, yellow).

In the CheA.P3-P4-P5 crystal structure (24), the ends of P4 helices and loops that are distal to the ATP-binding pocket (20) and P1 docking surfaces (23, 35) pack against the N and C termini of P3 helices in the same subunit (Fig. 7). In MD models of the core complex, residues in the linkers flanking the P4 domain pack against and probably stabilize the P3-P4 interface (19, 25; Cassidy et al., submitted). Mutational studies suggest that the two linkers may play different structure-function roles: An alanine replacement in L3 residue M322 or M326 reduced both basal and coupled CheA activity (19), whereas an alanine replacement at L4 residue L507, T508, or L509 produced little change in basal CheA activity but abrogated activation and control in core complexes (19). The structural basis for these activity changes is not yet clear, but the simplest possibility is that the P3-P4 interface is important for CheA activity and that lesions in the linkers destabilize that interface to various extents.

Linker mutants assemble core complexes, so their inability to activate implies that destabilization of the P3-L3-P4-L4 interface blocks the CheA catalytic cycle in core complexes (17–19). Conceivably, mutant-linker complexes could preferentially adopt the native, attractant-induced "off" conformation. However, it seems more likely that their CheA.P4 conformations are not sufficiently constrained to carry out the rapid reaction cycles characteristic of core complexes. L3 residue R325 forms a salt bridge with P4 residue D363 (19, 24; Cassidy et al., submitted) at the P3-P4 interface; a charge reversal at either member of the salt bridge pair also abrogates CheA activity and control (18, 19). These mutant studies indicate that L3, L4, and the P3-P4 interface are important for activation and downregulation of autophosphorylation activity in receptor core units. The L4 linker, in particular, may play a central role in transmitting receptor signals to the P3-L3-P4 interface via the CheW-CheA.P5-L4 linkage (17, 18, 36).

The dipped P4 conformation is critical for coupled CheA activity. In this study, we found that CheA residue R265, which lies at the N terminus of the P3 domain (Fig. 7), is critical for CheA function. All amino acid replacements examined at this position abrogated CheA activity and control in receptor signaling complexes. Charge reversals at R265 also impair basal CheA activity *in vitro* (R265E in this study; R265D in reference 19). In CheA dimers, R265 might facilitate a *trans* reaction between P1 and P4 (16, 25), but such a role cannot be critical to function because a stoichiometric excess of liberated P1 domains that lack a covalent connection to the catalytic center can support

chemoreceptor signaling (28). The R265E replacement disrupted chemotaxis in the liberated P1 system, demonstrating that R265 plays another, more critical signaling role (Fig. 4).

A salt bridge interaction between R265 and E368 characterizes the dipped P4 conformation seen in MD simulations (25). However, replacements at E368, which should abolish salt bridge formation with R265, did not abrogate CheA function. Similarly, replacements at D372 did not abolish CheA function. However, a doubly mutant E368A/D372A protein could not support kinase activity or chemotaxis. We suggest that either acidic residue can serve as a salt bridge partner for R265 to promote CheA signaling function, which implies that the kinase-active dipped P4 conformation may comprise a range of structural states. Our results also indicate that a polar interaction between CheA residue R265 and either E368 or D372 is sufficient for CheA activity and control in receptor core units; salt bridge formation is not essential. Although all R265 replacements (except R265K) impaired signaling function, the R265T and R265Q mutants regained chemotactic ability when combined with a polar replacement at either E368 or D372. These suppression effects were relatively modest but nevertheless suggest that H-bonding interactions among R265, E368, and D372 can promote the dipped P4 state needed for CheA activity and control in receptor core complexes.

Cassidy et al. (25) used disulfide formation between cysteine reporters in CheA and Tsr to confirm that the CheA.P4 domain can exist in both the dipped and undipped states *in vivo* (25). We obtained comparable results with the same cysteine reporter sites and the bifunctional cross-linking reagent bismaleimidoethane (BMOE). Although the distances between reporter pairs are very similar (25), the undipped reporters produced stronger cross-linking, suggesting, that the dipped conformation is relatively transient (25) and possibly more dynamic as well (this study). The Cys-containing Tsr and CheA reporter proteins support chemotaxis, indicating that the reporter residues themselves are not critical to CheA activation and control. Thus, with the exception of some charge reversals, which might be especially structure destabilizing, amino acid replacements at CheA-D316 (undipped), CheA-E361 (dipped), or Tsr-R394 (both conformations) failed to impair function. Given that the dipped state plays a critical role in receptor-coupled CheA activity, the Tsr-CheA dipped-state reporter pairs must contribute very little to the stability of that critical conformation.

Mechanisms of CheA control in receptor core complexes. *In vitro* studies of CheA signaling complexes in membranes (14, 37) and nanodiscs (14) have shown that receptors mainly modulate the catalytic rate constant of the autophosphorylation reaction. Subsequent network analyses revealed that dual regulation models involving control of ATP binding and either P1 binding or k_{cat} best fit the experimental data (38). The catalytically active dipped conformation could be the rate-limiting step in the overall reaction cycle. Accordingly, receptors in signaling complexes might enhance CheA activity by promoting the dipped state and might downregulate CheA by promoting the undipped state. Additionally, or alternatively, linkers L3 and L4 could directly propagate conformational changes to P4 helices involved in ATP or P1 binding or in catalysis (18; Cassidy et al., submitted).

The receptor-CheW-CheA.P5-L4 linkage could control CheA by modulating the P3/P3′/P4 packing arrangement to favor or hinder reaching the active, dipped P4 conformation. In cryo-ET analyses of mutant signaling complexes, off-shifted receptor complexes exhibit a large "keel" density below their hairpin tips (15, 39) that may correspond to P1 docked nonproductively to P4 in the undipped conformation. The signaling complexes of on-shifted receptors exhibit smaller keel volumes (15, 39), consistent with dynamic motion of P1, and possibly of P4, when CheA enters the dipped conformation.

We cannot yet say whether the undipped P4 conformation plays an active signaling role. On the one hand, the undipped P4 conformation could represent an essential step in a two-state reaction cycle. On the other hand, the undipped conformation could

simply correspond to the kinase-off state. It should be possible to distinguish these alternatives by identifying CheA residues that specifically promote the undipped conformation (Cassidy et al., submitted).

MATERIALS AND METHODS

Bacterial strains and plasmids. Strains used were derivatives of *E. coli* K-12 strain RP437 (40). Their names and relevant genotypes are as follows: UU2567 [Δ(*tar-cheZ*)4211 Δ(*tsr*)-5547 Δ*aer-1* Δ*trg-4543*]; UU2612 [Δ(*tar-tap*)4530 Δ*tsr-5547* Δ*aer-1* Δ*trg-4543*]; UU2683 [Δ(*cheA-cheW-tar-tap*)4530 Δ*aer-1* Δ*trg-4543*]; UU2784 [Δ(*cheA-cheW-tar-tap-cheR-cheB-cheY-cheZ*)1214 Δ*aer-1* Δ*trg-4543*]; UU2806 [Δ(*cheA-cheW-tar-tap-cheR-cheB-cheY-cheZ*)1214 Δ*tsr-5547* Δ*aer-1* Δ*trg-4543*]; and UU2960 [Δ(*cheA-cheW-tar-tap-cheR-cheB*)1350 Δ(*tsr*)-5547 Δ*aer-1* Δ*trg-4543*]. The plasmids used in this work are listed in Table S4 in the supplemental material.

Site-directed mutagenesis. Mutations were generated in various plasmids carrying the *cheA* or *tsr* genes with the Agilent QuikChange II site-directed mutagenesis kit and confirmed by DNA sequencing of the entire coding region of the targeted gene(s).

Chemotaxis assays. The chemotactic ability of CheA mutants was assessed in strain U2683 transformed with pPM25 derivatives; Tsr mutants were studied in UU2612 transformed with pRR53 derivatives. Individual colonies of UU2683 bearing pPM25 derivatives were inoculated in tryptone soft agar plates (10 g/liter tryptone, 5 g/liter NaCl, and 2.5 g/liter agar) supplemented with 12.5 μg/ml chloramphenicol and 0.6 μM sodium salicylate. Individual colonies of UU2612 bearing pRR53 derivatives were inoculated in tryptone soft agar plates supplemented with 50 μg/ml ampicillin and 100 μM IPTG. Plates were incubated at 32.5°C for 7 h before imaging.

Chemotaxis by P3-P4-P5 CheA was determined in strain UU2683 cotransformed with plasmid pGP67 (and derivative mutants) and pAG17. Cells were inoculated in tryptone soft agar plates (10 g/liter tryptone, 5 g/liter NaCl, 2.5 g/liter agar) supplemented with 12.5 μg/ml chloramphenicol, 0.6 μM sodium salicylate, 50 μg/ml ampicillin, and 1 mM IPTG. Plates were incubated at 32.5°C for 10 h before imaging.

Expression levels of mutant CheA proteins. Strain UU2683 harboring plasmid pPM25 and its mutant derivatives was grown at 30°C in tryptone broth supplemented with 12.5 μg/ml chloramphenicol and 0.6 μM sodium salicylate to the mid-exponential phase. A 1-ml culture aliquot was centrifuged, and cells were resuspended and lysed in 100 μl of 1× Laemmli sample buffer (41). CheA protein was visualized and quantified by Western blotting with a polyclonal rabbit CheA antiserum.

Expression levels of mutant Tsr proteins. Strain UU2610 harboring plasmid pRR53 and its mutant derivatives was grown to the mid-exponential phase at 30°C in tryptone broth supplemented with 100 μg/ml ampicillin and 100 μM IPTG. A 1-ml culture aliquot was centrifuged, and cells were resuspended and lysed in 100 μl of 1× Laemmli sample buffer (41). Tsr protein was visualized and quantified by Western blotting with a polyclonal rabbit Tsr antiserum.

***In vivo* FRET-based CheA kinase assays.** The experimental system, cell sample chamber, stimulus protocol, and data analysis followed the hardware, software, and methods originally described by Sourjik et al. (42) with minor modifications (33). CheA mutants were studied in strain UU2784 bearing the FRET reporter plasmid pVS88 and a pPM25 derivative. Tsr mutants were analyzed in strain UU2567 cotransformed with pRZ30 and a pRR53 derivative. Cells of strain UU2784 were grown at 30°C in tryptone broth (10 g/liter tryptone, 5 g/liter NaCl) supplemented with 12.5 μg/ml chloramphenicol, 50 μg/ml ampicillin, 50 μM IPTG, and 0.6 μM sodium salicylate, whereas UU2567 cells were cultured in tryptone broth supplemented with 12.5 μg/ml chloramphenicol, 50 μg/ml ampicillin, 100 μM IPTG, and 2 μM sodium salicylate. When cells reached the mid-exponential phase (optical density at 600 nm [OD$_{600}$], ~0.5), they were washed twice with motility buffer (10 mM potassium phosphate, 0.1 mM EDTA, and 10 mM lactic acid [pH 7]) containing 100 μM L-methionine, resuspended in 50 μl of motility buffer, and attached to a round poly-D-lysine-coated coverslip that was later mounted in a flow cell (43). Cells were subjected to sequential addition and removal of serine diluted in motility buffer and kept at 30°C throughout the experiment. Photon-counting photomultipliers were used to measure the epifluorescent light emitted by CFP (FRET donor) and YFP (FRET acceptor) from the cell sample excited at the CFP wavelength. The ratio of YFP to CFP photon counts, which reflects CheA kinase activity and changes in response to serine stimuli, was recorded over time (26, 42). Dose-response curves were obtained by plotting the fractional changes in kinase activity versus applied serine concentrations. Data were fitted to a multisite Hill equation, $1 - [Ser]^H/([Ser]^H + K_{1/2}{}^H)$, where $K_{1/2}$ is the concentration of attractant that inhibits 50% of the kinase activity and H, the Hill coefficient, reflects the cooperativity of the response. Total CheA kinase activity was calculated as the larger of the FRET changes elicited by a saturating serine stimulus or by 3 mM KCN.

Phenotypic suppression analysis. To find suppressors of CheA R265 mutants, residues E368 and D372 were subjected, individually or simultaneously, to site-directed mutagenesis (QuikChange II; Agilent Technologies) with degenerate primers in pPM25 derivatives already bearing R265E, L, T, or Q mutations. QuikChange reaction products were electroporated into strain UU2683 and seeded in the middle of a tryptone soft agar plate supplemented with 12.5 μg/ml chloramphenicol and 0.6 μM sodium salicylate. Plates were incubated overnight at 30°C to allow the appearance of chemotactic revertants.

Protein expression and purification. CheA and CheY, both bearing an N-terminal 8×His and Twin-Strep-tag (HTS tag; IBA Lifesciences) were purified from strain UU2806 transformed with pGP59 (HTS-CheA) and strain BL21(DE3) transformed with pGP65 (HTS-CheY). *E. coli* cells were grown at 37°C with agitation (250 rpm) in 800 ml of Terrific broth (12 g/liter tryptone, 24 g/liter yeast extract, 0.4% [vol/vol] glycerol, 17 mM KH$_2$PO$_4$, and 72 mM K$_2$HPO$_4$) supplemented with 100 μg/ml ampicillin until an

OD_{600} of ~0.4 was reached, at which time 1 mM IPTG was added. Cultures were further incubated for 6 h at 37°C with agitation (250 rpm). Soluble proteins were purified from clarified protein lysates obtained by sonication according to the two-step affinity purification protocol (Qiagen). Proteins were concentrated by ultrafiltration using a Centricon YM-10 (for HTS-CheY) or YM30 (for HTS-CheA) centrifugal filter unit (Millipore) and dialyzed against storage buffer (50 mM Tris, 1 mM dithiothreitol (DTT), 10% [vol/vol] glycerol [pH 7.5]). Samples were snap-frozen in dry ice and stored at −70°C until use. Protein purity was ≥95% as determined by SDS-PAGE followed by SYPRO Ruby staining (Invitrogen). Protein concentrations were determined from SYPRO Ruby-stained polyacrylamide gels as well as from UV absorption using the 280-nm extinction coefficients calculated from protein sequences, namely, 28.4 and 19.5 $mM^{-1} \cdot cm^{-1}$ for CheA and CheY, respectively.

Determination of CheA basal kinase activity. Free CheA autophosphorylation rates were determined with an enzymatically coupled assay that determines ATP hydrolysis by monitoring NADH decay as previously described (19). The assay was done at room temperature, with 2 μM CheA and 50 μM CheY in kinase buffer (50 mM Tris, 50 mM KCl, 5 mM $MgCl_2$, 0.1 mM DTT, 1.5 mM ATP, 1.5 mM PEP, 0.25 mM NADH, 0.06 U/μl pyruvate kinase, 0.075 U/μl lactate dehydrogenase, pH 7.5). Under these conditions CheA autophosphorylation rate was 700 ± 100 nM/min ($n = 3$).

***In vivo* cross-linking methods.** To test CheA-P4 conformations, strain UU2960 bearing plasmid pRR53-R394C was transformed either with pGP57-D316C or pGP57-E361C and their respective mutant derivatives. Cultures were grown at 30°C with agitation (250 rpm) in tryptone broth supplemented with 12.5 μg/ml chloramphenicol, 50 μg/ml ampicillin, 150 μM IPTG, and 0.6 μM sodium salicylate. At an OD_{600} of ~0.5, 1.5 ml of the culture was withdrawn and subjected to two washing steps that consisted of centrifugation at 6,000 × g for 5 min at room temperature and resuspension in 1 ml of phosphate-buffered saline (PBS). Cells were kept at 30°C for 10 min, and cross-linking of samples was initiated with 200 μM bismaleimidoethane (BMOE) and stopped with 10 mM N-ethylmaleimide (NEM) after 10 s. Samples were centrifuged at 21,000 × g for 3 min and lysed in 50 μl of 2× Laemmli sample loading buffer. HA-tagged CheA and derivative cross-linked species were detected by Western blotting using a polyclonal antihemagglutinin (anti-HA) antibody (Pierce).

The effect of CheA mutants on CheA-CheW interfaces was evaluated in UU2806 cells cotransformed with pRR53 and a compatible plasmid expressing either interface 1 (pGP58) or interface 2 (pGP55) cross-linking reporter proteins. Cultures were grown at 30°C with agitation (250 rpm) in tryptone broth supplemented with 12.5 μg/ml chloramphenicol, 50 μg/ml ampicillin, 50 μM IPTG, and 0.6 μM sodium salicylate to an OD_{600} of ~0.5. Cells were treated with 300 μM Cu^{2+} for 10 min at 35°C to induce disulfide formation, and HA-tagged CheA and its cross-linking product with CheW was detected by Western blotting using a polyclonal anti-HA antibody (Pierce) as previously described (9).

CheA clustering assays. Strain UU2806 cotransformed with plasmid pRR53 and pAV232 (and derivative mutant plasmids) was grown at 30°C with agitation (250 rpm) in tryptone broth supplemented with 12.5 μg/ml chloramphenicol, 50 μg/ml ampicillin, 100 μM IPTG, and 0.6 μM sodium salicylate to an OD_{600} of ~0.5. Cells were washed twice with motility buffer, attached to a poly-lysine-coated coverslip and analyzed by fluorescence microscopy as previously described (32).

Protein structural display. MacPyMOL was used to display the atomic coordinates of a core signaling unit from *Thermotoga maritima* exhibiting Che.P4 domains in both open and closed conformations (25).

SUPPLEMENTAL MATERIAL

Supplemental material for this article may be found at https://doi.org/10.1128/JB.00543-19.

SUPPLEMENTAL FILE 1, PDF file, 0.4 MB.

ACKNOWLEDGMENTS

REFERENCES

1. Quezada CM, Hamel DJ, Grădinaru C, Bilwes AM, Dahlquist FW, Crane BR, Simon MI. 2005. Structural and chemical requirements for histidine phosphorylation by the chemotaxis kinase CheA. J Biol Chem 280:30581–30585. https://doi.org/10.1074/jbc.M505316200.
2. Bourret RB, Hess JF, Simon MI. 1990. Conserved aspartate residues and phosphorylation in signal transduction by the chemotaxis protein CheY. Proc Natl Acad Sci U S A 87:41–45. https://doi.org/10.1073/pnas.87.1.41.
3. Welch M, Oosawa K, Aizawa S, Eisenbach M. 1993. Phosphorylation-dependent binding of a signal molecule to the flagellar switch of bacteria. Proc Natl Acad Sci U S A 90:8787–8791. https://doi.org/10.1073/pnas.90.19.8787.
4. Blat Y, Eisenbach M. 1994. Phosphorylation-dependent binding of the chemotaxis signal molecule CheY to its phosphatase, CheZ. Biochemistry 33:902–906. https://doi.org/10.1021/bi00170a008.
5. Parkinson JS, Hazelbauer GL, Falke JJ. 2015. Signaling and sensory

adaptation in *Escherichia coli* chemoreceptors: 2015 update. Trends Microbiol 23:257–266. https://doi.org/10.1016/j.tim.2015.03.003.

6. Li M, Hazelbauer GL. 2011. Core unit of chemotaxis signaling complexes. Proc Natl Acad Sci U S A 108:9390–9395. https://doi.org/10.1073/pnas.1104824108.

7. Briegel A, Li X, Bilwes AM, Hughes KT, Jensen GJ, Crane BR. 2012. Bacterial chemoreceptor arrays are hexagonally packed trimers of receptor dimers networked by rings of kinase and coupling proteins. Proc Natl Acad Sci U S A 109:3766–3771. https://doi.org/10.1073/pnas.1115719109.

8. Liu J, Hu B, Morado DR, Jani S, Manson MD, Margolin W. 2012. Molecular architecture of chemoreceptor arrays revealed by cryoelectron tomography of *Escherichia coli* minicells. Proc Natl Acad Sci U S A 109: E1481–E1488. https://doi.org/10.1073/pnas.1200781109.

9. Pinas GE, Frank V, Vaknin A, Parkinson JS. 2016. The source of high signal cooperativity in bacterial chemosensory arrays. Proc Natl Acad Sci U S A 113:3335–3340. https://doi.org/10.1073/pnas.1600216113.

10. Swanson RV, Bourret RB, Simon MI. 1993. Intermolecular complementation of the kinase activity of CheA. Mol Microbiol 8:435–441. https://doi.org/10.1111/j.1365-2958.1993.tb01588.x.

11. Levit M, Liu Y, Surette M, Stock J. 1996. Active site interference and asymmetric activation in the chemotaxis protein histidine kinase CheA. J Biol Chem 271:32057–32063. https://doi.org/10.1074/jbc.271.50.32057.

12. Borkovich KA, Kaplan N, Hess JF, Simon MI. 1989. Transmembrane signal transduction in bacterial chemotaxis involves ligand-dependent activation of phosphate group transfer. Proc Natl Acad Sci U S A 86: 1208–1212. https://doi.org/10.1073/pnas.86.4.1208.

13. Bourret RB, Davagnino J, Simon MI. 1993. The carboxy-terminal portion of the CheA kinase mediates regulation of autophosphorylation by transducer and CheW. J Bacteriol 175:2097–2101. https://doi.org/10.1128/jb.175.7.2097-2101.1993.

14. Pan W, Dahlquist FW, Hazelbauer GL. 2017. Signaling complexes control the chemotaxis kinase by altering its apparent rate constant of autophosphorylation. Protein Sci 26:1535–1546. https://doi.org/10.1002/pro.3179.

15. Briegel A, Ames P, Gumbart JC, Oikonomou CM, Parkinson JS, Jensen GJ. 2013. The mobility of two kinase domains in the *Escherichia coli* chemoreceptor array varies with signalling state. Mol Microbiol 89:831–841. https://doi.org/10.1111/mmi.12309.

16. Greenswag AR, Muok A, Li X, Crane BR. 2015. Conformational transitions that enable histidine kinase autophosphorylation and receptor array integration. J Mol Biol 427:3890–3907. https://doi.org/10.1016/j.jmb.2015.10.015.

17. Ding X, He Q, Shen F, Dahlquist FW, Wang X. 2018. Regulatory role of an interdomain linker in the bacterial chemotaxis histidine kinase CheA. J Bacteriol 200:e00052-18. https://doi.org/10.1128/JB.00052-18.

18. Wang X, Vallurupalli P, Vu A, Lee K, Sun S, Bai WJ, Wu C, Zhou H, Shea JE, Kay LE, Dahlquist FW. 2014. The linker between the dimerization and catalytic domains of the CheA histidine kinase propagates changes in structure and dynamics that are important for enzymatic activity. Biochemistry 53:855–861. https://doi.org/10.1021/bi4012379.

19. Wang X, Wu C, Vu A, Shea JE, Dahlquist FW. 2012. Computational and experimental analyses reveal the essential roles of interdomain linkers in the biological function of chemotaxis histidine kinase CheA. J Am Chem Soc 134:16107–16110. https://doi.org/10.1021/ja3056694.

20. Bilwes AM, Quezada CM, Croal LR, Crane BR, Simon MI. 2001. Nucleotide binding by the histidine kinase CheA. Nat Struct Biol 8:353–360. https://doi.org/10.1038/86243.

21. Gloor SL, Falke JJ. 2009. Thermal domain motions of CheA kinase in solution: disulfide trapping reveals the motional constraints leading to trans-autophosphorylation. Biochemistry 48:3631–3644. https://doi.org/10.1021/bi900033r.

22. Hamel DJ, Zhou H, Starich MR, Byrd RA, Dahlquist FW. 2006. Chemical-shift-perturbation mapping of the phosphotransfer and catalytic domain interaction in the histidine autokinase CheA from *Thermotoga maritima*. Biochemistry 45:9509–9517. https://doi.org/10.1021/bi060798k.

23. Zhang J, Xu Y, Shen J, Luo X, Chen J, Chen K, Zhu W, Jiang H. 2005. Dynamic mechanism for the autophosphorylation of CheA histidine kinase: molecular dynamics simulations. J Am Chem Soc 127: 11709–11719. https://doi.org/10.1021/ja051199o.

24. Bilwes AM, Alex LA, Crane BR, Simon MI. 1999. Structure of CheA, a signal-transducing histidine kinase. Cell 96:131–141. https://doi.org/10.1016/s0092-8674(00)80966-6.

25. Cassidy CK, Himes BA, Alvarez FJ, Ma J, Zhao G, Perilla JR, Schulten K, Zhang P. 2015. CryoEM and computer simulations reveal a novel kinase conformational switch in bacterial chemotaxis signaling. Elife 4:e08419. https://doi.org/10.7554/eLife.08419.

26. Sourjik V, Berg HC. 2002. Receptor sensitivity in bacterial chemotaxis. Proc Natl Acad Sci U S A 99:123–127. https://doi.org/10.1073/pnas.011589998.

27. Sourjik V, Berg HC. 2004. Functional interactions between receptors in bacterial chemotaxis. Nature 428:437–441. https://doi.org/10.1038/nature02406.

28. Garzon A, Parkinson JS. 1996. Chemotactic signaling by the P1 phosphorylation domain liberated from the CheA histidine kinase of *Escherichia coli*. J Bacteriol 178:6752–6758. https://doi.org/10.1128/jb.178.23.6752-6758.1996.

29. Jahreis K, Morrison TB, Garzon A, Parkinson JS. 2004. Chemotactic signaling by an *Escherichia coli* CheA mutant that lacks the binding domain for phosphoacceptor partners. J Bacteriol 186:2664–2672. https://doi.org/10.1128/JB.186.9.2664-2672.2004.

30. Stewart RC, Jahreis K, Parkinson JS. 2000. Rapid phosphotransfer to CheY from a CheA protein lacking the CheY-binding domain. Biochemistry 39:13157–13165. https://doi.org/10.1021/bi001100k.

31. Natale AM, Duplantis JL, Piasta KN, Falke JJ. 2013. Structure, function, and on-off switching of a core unit contact between CheA kinase and CheW adaptor protein in the bacterial chemosensory array: a disulfide mapping and mutagenesis study. Biochemistry 52:7753–7765. https://doi.org/10.1021/bi401159k.

32. Ames P, Studdert CA, Reiser RH, Parkinson JS. 2002. Collaborative signaling by mixed chemoreceptor teams in *Escherichia coli*. Proc Natl Acad Sci U S A 99:7060–7065. https://doi.org/10.1073/pnas.092071899.

33. Lai RZ, Parkinson JS. 2014. Functional suppression of HAMP domain signaling defects in the *E. coli* serine chemoreceptor. J Mol Biol 426: 3642–3655. https://doi.org/10.1016/j.jmb.2014.08.003.

34. Park SY, Borbat PP, Gonzalez-Bonet G, Bhatnagar J, Pollard AM, Freed JH, Bilwes AM, Crane BR. 2006. Reconstruction of the chemotaxis receptor-kinase assembly. Nat Struct Mol Biol 13:400–407. https://doi.org/10.1038/nsmb1085.

35. Nishiyama S, Garzon A, Parkinson JS. 2014. Mutational analysis of the P1 phosphorylation domain in *Escherichia coli* CheA, the signaling kinase for chemotaxis. J Bacteriol 196:257–264. https://doi.org/10.1128/JB.01167-13.

36. Pinas GE, DeSantis MD, Parkinson JS. 2018. Noncritical signaling region of a kinase-receptor interaction surface in the *Escherichia coli* chemosensory core complex. J Mol Biol 430:1051–1064. https://doi.org/10.1016/j.jmb.2018.02.004.

37. Levit MN, Liu Y, Stock JB. 1999. Mechanism of CheA protein kinase activation in receptor signaling complexes. Biochemistry 38:6651–6658. https://doi.org/10.1021/bi982839l.

38. Mello BA, Pan W, Hazelbauer GL, Tu Y. 2018. A dual regulation mechanism of histidine kinase CheA identified by combining network-dynamics modeling and system-level input-output data. PLoS Comput Biol 14:e1006305. https://doi.org/10.1371/journal.pcbi.1006305.

39. Yang W, Cassidy CK, Ames P, Diebolder CA, Schulten K, Luthey-Schulten Z, Parkinson JS, Briegel A. 2019. *In situ* conformational changes of the *Escherichia coli* serine chemoreceptor in different signaling states. mBio 10. https://doi.org/10.1128/mBio.00973-19.

40. Parkinson JS, Houts SE. 1982. Isolation and behavior of *Escherichia coli* deletion mutants lacking chemotaxis functions. J Bacteriol 151:106–113.

41. Laemmli UK. 1970. Cleavage of structural proteins during the assembly of the head of bacteriophage T4. Nature 227:680–685. https://doi.org/10.1038/227680a0.

42. Sourjik V, Vaknin A, Shimizu TS, Berg HC. 2007. *In vivo* measurement by FRET of pathway activity in bacterial chemotaxis. Methods Enzymol 423:365–391. https://doi.org/10.1016/S0076-6879(07)23017-4.

43. Berg HC, Block SM. 1984. A miniature flow cell designed for rapid exchange of media under high-power microscope objectives. J Gen Microbiol 130: 2915–2920. https://doi.org/10.1099/00221287-130-11-2915.

SUPPLEMENTAL MATERIALS
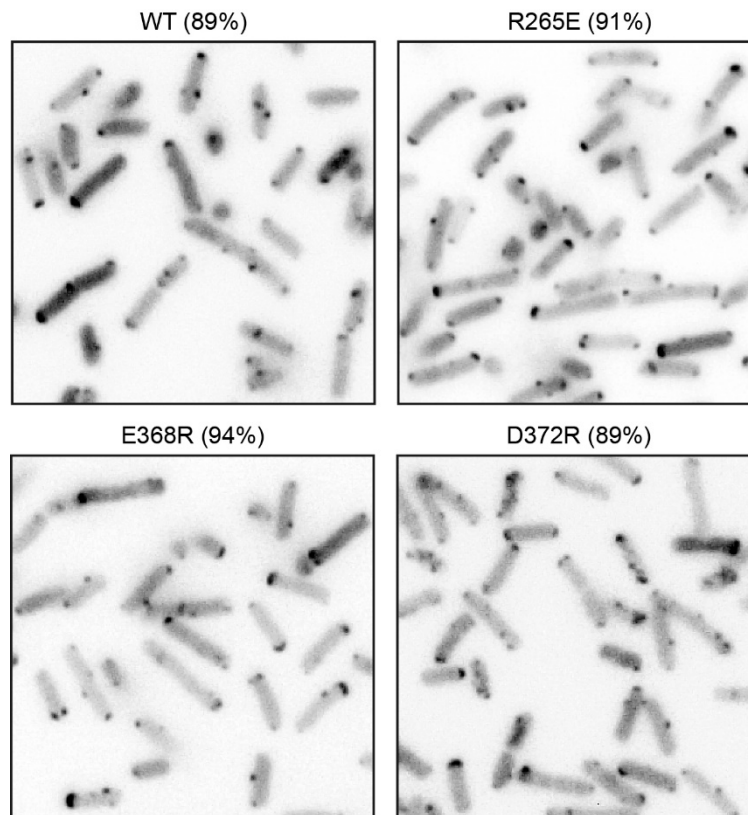
Fig. S1

Fig. S1. Array formation by CheA charge reversal mutants. Plasmid pAV232 derivatives encoding CheA::mYFP CheW in combination with a charge reversal at the indicated CheA residues were induced at 0.6 μM sodium salicylate in strain UU2806 expressing Tsr from plasmid pRR53. Fluorescence images were converted to grayscale and inverted to enhance visualization of receptor clusters (dark spots, typically at the cell poles). For each test, 100 cells were examined. Values indicate the percentage of cells with one or more discernable clusters.

Fig. S2

A

array interface 2
CheW-E27C x CheA*-A546C

WT   R265E E368R D372R

CheA~CheW ▶
CheA ▷

B

array interface 1
CheW-Q44C x CheA*-S630C

WT   R265E E368R D372R

CheA~CheW ▶
CheA ▷

interface 1 controls

CheA: WT   L633A   WT   L633A
CheW: WT   WT   K56I K56I
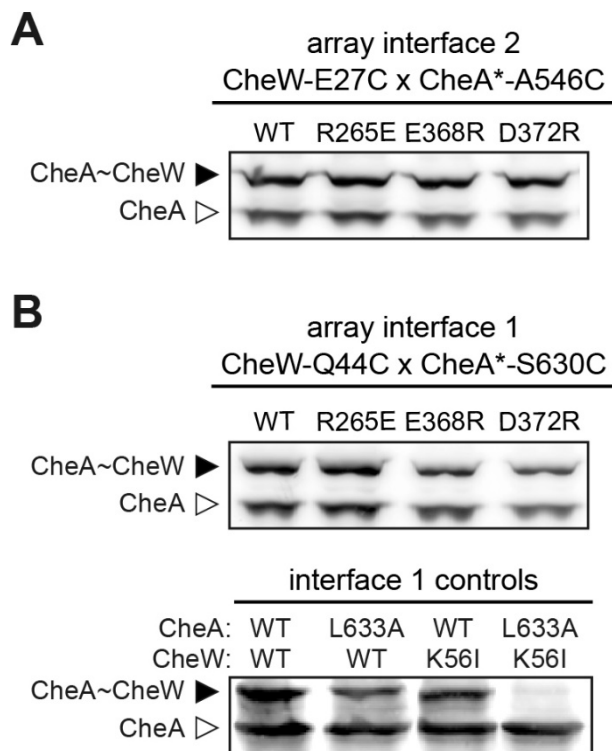
CheA~CheW ▶
CheA ▷

Fig. S2. Crosslinking at array interfaces 1 and 2 in CheA charge-reversal mutants. CheA-CheW proteins bearing cysteine reporters for interface 1 or 2 and the indicated charge reversal lesions were induced from plasmid pGP55 with 0.6 μM sodium salicylate in strain UU2806 bearing plasmid pRR53 to supply wild-type Tsr. Cells were treated with 300 μM Cu^{2+} for 10 min at 35 °C to induce disulfide formation. Whole cell lysates were separated by SDS/PAGE; HA-tagged CheA and its crosslinking product with CheW were detected by immunoblotting with a polyclonal anti-HA antibody.

(A) Interface 2 crosslinking reporters CheA-A546C/CheW-E27C were validated in a previous report (1)

(B) Interface 1 crosslinking reporters. CheA-S630C/CheW-Q44C (2). CheA-L633A and/or CheW-K56I lesions in the reporter proteins served as controls to validate specificity of the interface 1 assay. Only the double-mutant combination abrogated the interface 1 cross-linking signal.

Table S1. Signaling properties of CheA-E368*–CheA-R265*–CheA-D372*

CheA mutant	relative taxis[a]	relative [CheA*][b]	$K_{1/2}$ (µM SER)[c]	Hill coefficient[c]	relative activity[d]
R265A	0.10	0.86	NR	NR	0.24
R265E	0.10	0.77	NR	NR	0.14
R265G	0.10	0.83	NR	NR	0.21
R265K	0.42	0.76	13 ± 1	6 ± 1	0.8 ± 0.1
R265L	0.10	0.79	NR	NR	0.14
R265Q	0.10	0.77	NR	NR	0.16
R265T	0.10	0.70	NR	NR	0.24
E368A	0.59	0.96	12	6.8	0.50 ± 0.05
E368D	0.35	0.85	10	18	0.5 ± 0.1
E368G	0.21	0.86	12 ± 1	7 ± 2	0.38 ± 0.05
E368K	0.13	0.81	5.3	1.8	0.26 ± 0.08
E368L	0.12	1.08	13	12	0.4 ± 0.1
E368Q	0.89	0.91	13	26	1.05
E368R	0.12	0.78	NR	NR	0.22
E368S	0.40	nd	13	10	0.33
E368T	0.25	1.01	9.9 ± 0.1	7 ± 2	0.3 ± 0.1
D372A	0.63	1.00	16	14	0.5 ± 0.1
D372E	0.53	0.78	13	7.2	0.5 ± 0.1
D372F	0.56	nd	15	8.6	0.19
D372G	0.51	1.03	12	9.5	0.31 ± 0.01
D372K	0.09	0.80	NR	NR	0.09
D372L	0.40	1.00	16	16	0.34 ± 0.08
D372N	0.66	0.99	16	10	0.5 ± 0.1
D372R	0.10	1.19	NR	NR	0.10
D372S	0.77	nd	14	14	0.31
D372T	0.46	0.92	12	13	0.80 ± 0.07
E368A/D372A	0.11	0.89	NR	NR	0.16
R265Q/E368Q	0.22	nd	9.9	18	0.34
R265Q/D372S	0.32	nd	14	13	0.39
R265Q/D372T	0.20	nd	12	11	0.26

continued below...

R265T/E368Q	nd	0.26	12	6.9	0.29
R265T/D372S	nd	0.46	14	9.3	0.33
R265T/D372T	nd	0.31	14	8.9	0.24
R265T/D372N	nd	0.18	12	9	0.30
R265Q/E368Q/D372S	nd	0.51	14	12	0.26
R265T/E368Q/D372N	nd	0.33	16	27	0.39

[a] Size of mutant pPM25*/UU2683 colony relative to wild-type on tryptone soft agar after incubation at 30°C for 8 hours (see Methods for details).

[b] Expression level of mutant CheA protein relative to wild-type (see Methods for details).

[a] Data from FRET-based dose-response experiments (see Methods for details). Values below 10 are rounded to the nearest 0.1; values above 10 are rounded to the nearest whole number. Values with errors represent averages and standard deviations of two or more measurements. Wild-type responses to serine had a $K_{1/2}$ of 17 ± 1 μM and a Hill coefficient of 18 ± 3. NR: no detectable response to 10 mM serine.

[d] Maximal activity in FRET kinase assays, based either on a saturating serine response (3) or, if no serine response, on the FRET drop upon treatment with 3 mM KCN (4). Values with errors represent averages and standard deviations of two or more measurements.

Table S2. Suppressors of CheA-R265T or -R265Q mutants at CheA residues E368 and D372

Residue at CheA position:			Chemotaxis	Residue at CheA position:			Chemotaxis
R265	**E368**	**D372**	Function[a]	**R265**	**E368**	**D372**	Function[a]
+	+	+	1	Q	C	+	0.11
+	+	A	0.63	Q	L	+	0.08
+	+	L	0.35	Q	N	+	0.08
+	+	M	0.38	Q	Q	+	0.22
+	+	N	0.59	Q	T	+	0.09
+	+	S	0.57	Q	Q	A	0.24
+	+	T	0.42	Q	Q	M	0.28
+	A	+	0.45	Q	C	S	0.35
+	C	+	0.50	Q	N	S	0.27
+	L	+	0.15	Q	Q	S	0.51
+	N	+	0.17	Q	T	S	0.37
+	Q	+	0.89	Q	L	T	0.26
+	R	+	0.10	Q	T	T	0.27
+	S	+	0.45	T	+	+	0.08
+	T	+	0.18	T	+	A	0.10
+	A	S	0.09	T	+	L	0.08
+	C	S	0.37	T	+	M	0.07
+	L	S	0.07	T	+	N	0.18
+	L	T	0.29	T	+	S	0.46
+	N	S	0.14	T	+	T	0.31
+	Q	A	0.39	T	A	+	0.09
+	Q	L	0.35	T	L	+	0.09
+	Q	M	0.51	T	Q	+	0.26
+	Q	N	0.41	T	R	+	0.15
+	Q	S	0.57	T	S	+	0.10
+	R	S	0.12	T	T	+	0.09
+	S	S	0.20	T	Q	A	0.31
+	T	S	0.34	T	Q	L	0.19
+	T	T	0.33	T	Q	M	0.27
Q	+	+	0.09	T	Q	N	0.33
Q	+	A	0.08	T	A	S	0.26
Q	+	M	0.08	T	L	S	0.31
Q	+	S	0.32	T	R	S	0.27
Q	+	T	0.20	T	S	S	0.36
				T	T	S	0.43

[a] Fraction of wild-type colony diameter on tryptone soft agar plates.

Table S3. Signaling properties of CheA-D316*–Tsr-R394*–CheA-E361*

CheA mutant	relative [CheA*][b]	relative taxis[a]	$K_{1/2}$ (µM SER)[c]	Hill coefficient[c]	relative activity[d]
D316A	1.07	0.94	12	16	0.78
D316C	1.12	0.76	13	3.0	0.81
D316E	1.12	0.83	15	14	1.0 ± 0.2
D316G	1.30	0.87	14	16	1.19
D316K	1.08	0.95	12	16	0.76
D316L	0.98	0.99	13	20	1.33
D316N	1.10	0.71	11	18	0.90
D316R	0.98	0.38	11 ± 1	4.7 ± 0.6	1.19
D316T	1.14	0.73	11	16	1.17
E361A	0.53	0.36	18	23	0.95
E361C	1.26	0.35	nd	nd	0.79
E361D	1.20	0.64	11	18	0.9 ± 0.1
E361G	0.63	0.76	11	13	0.86
E361K	1.12	0.37	13	14	1.0 ± 0.2
E361L	0.79	0.39	11	21	0.9 ± 0.2
E361Q	1.30	0.32	22	27	0.7 ± 0.2
E361R	0.78	0.34	16	7.0	0.6 ± 0.1
E361T	1.30	0.67	13	13	0.8 ± 0.1

Tsr mutant	relative [Tsr*][f]	relative taxis[e]	$K_{1/2}$ (µM SER)[c]	Hill coefficient[c]	relative activity[d]
R394A	0.91	0.36	1.4	13	0.76
R394C	0.75	0.38	1.6	7.1	1.73
R394D	0.69	0.49	4.8	9.7	1.24
R394E	0.73	0.09	0.3	1.6	0.48 ± 0.09
R394G	1.04	0.11	NR	NR	0.32
R394K	1.14	0.56	16	12	1.16
R394L	0.93	0.42	2.9	9.3	0.95
R394Q	0.89	0.32	0.9	6.9	0.78
R394T	0.96	0.43	0.7	5.5	1.46

continued below...

[a] Size of mutant pPM25*/UU2683 colony relative to wild-type on tryptone soft agar after
incubation at 30°C for 8 hours (see Methods for details).

[b] Expression level of mutant CheA protein relative to wild-type (see Methods for details).

[c] Data from FRET-based dose-response experiments (see Methods for details). Values below
10 are rounded to the nearest 0.1; values above 10 are rounded to the nearest whole number.
Values with errors represent averages and standard deviations of two or more measurements.
Wild-type responses to serine had a $K_{1/2}$ of 17 ±1 μM and a Hill coefficient of 18 ± 3. NR: no
detectable response to 10 mM serine.

[d] Maximal activity relative to wild type in FRET kinase assays, based either on a saturating
serine response (3) or, if no serine response, on the FRET drop upon treatment with 3 mM
KCN (4). Values with errors represent averages and standard deviations of two or more
measurements.

Table S4. Plasmids

Plasmid	Properties or genotype of expression insert	Reference
Group 1	derivatives of pBR322; confer ampicillin resistance; stringent colE1 replication system; IPTG-inducible P$_{tac}$ expression vectors	
pRR48	vector, low-expression	(5)
pNP1	vector, high-expression	(6)
pCJ30	vector, high-expression	(7)
pRR53	pRR48 derivative; *tsr$^+$*	(5)
pGP59	pNP1 derivative; *N-terminal [a]HTS-tagged cheA*	this study
pAG17	pCJ30 derivative*; cheA(1-141)*	(8)
Group 2	derivatives of pACYC184; confer chloramphenicol resistance; p15A replication system; sodium salicylate-inducible expression	(9, 10)
pKG116	vector	(11)
pPM25	pKG116 derivative; *cheA$^+$ cheW$^+$*	(1)
pRZ30	pKG116 derivative; *cheY-yfp cheZ-cfp*	(4)
pAV232	pPM25 derivative; *cheA(Δ[161-226]Ωmyfp) cheW$^+$*	(1)
pGP57	pPM25 derivative; *cheA(M98L/C120S/C213S/C415S) cheA(S2ΩHA[b]) cheW$^+$*	this study
pGP55	pPM25 derivative; *cheA(M98L/C120S/C213S/C415S/A546C) cheA(S147ΩHA/A241ΩHA) cheW(E27C)*	(1)
pGP58	pPM25 derivative; *cheA(M98L/C120S/C213S/C415S/S630C) cheA(S147ΩHA/A241ΩHA) cheW(Q44C)*	this study
pGP67	pPM25 derivative; *cheAΔ(7-247) cheW$^+$*	this study

Group 3	Derivatives of pUC19; confer ampicillin resistance; relaxed colE1 replication system; IPTG-inducible P$_{T7}$ expression vectors	
pRSET-A	vector	Invitrogen
pGP65	pRSET-A derivative; *N-terminal HTS-tagged cheY*	this study
Group 4	derivatives of pUC18; confer ampicillin resistance; relaxed colE1 replication system; IPTG-inducible P$_{trc}$ expression vectors	
pTrc99A	vector	(12)
pVS88	pTrc99A derivative, *cheY-yfp cheZ-cfp*	(13)

[a] HTS, 8X-His/Twin-Strep® tag: HHHHHHHGGSWSHPQFEKGGGSGGGSGGSAWSHPQFEK

[b] HA, HA tag: YPYDVPDYA

REFERENCES

1. Pinas GE, Frank V, Vaknin A, Parkinson JS. 2016. The source of high signal cooperativity in bacterial chemosensory arrays. Proc Natl Acad Sci U S A 113:3335-40.

2. Natale AM, Duplantis JL, Piasta KN, Falke JJ. 2013. Structure, function, and on-off switching of a core unit contact between CheA kinase and CheW adaptor protein in the bacterial chemosensory array: A disulfide mapping and mutagenesis study. Biochemistry 52:7753-65.

3. Sourjik V, Vaknin A, Shimizu TS, Berg HC. 2007. In vivo measurement by FRET of pathway activity in bacterial chemotaxis. Methods Enzymol 423:365-91.

4. Lai RZ, Parkinson JS. 2014. Functional suppression of HAMP domain signaling defects in the E. coli serine chemoreceptor. J Mol Biol 426:3642-55.

5. Studdert CA, Parkinson JS. 2005. Insights into the organization and dynamics of bacterial chemoreceptor clusters through in vivo crosslinking studies. Proc Natl Acad Sci U S A 102:15623-8.

6. Bibikov SI, Miller AC, Gosink KK, Parkinson JS. 2004. Methylation-independent aerotaxis mediated by the Escherichia coli Aer protein. J Bacteriol 186:3730-7.

7. Bibikov SI, Biran R, Rudd KE, Parkinson JS. 1997. A signal transducer for aerotaxis in Escherichia coli. J Bacteriol 179:4075-9.

8. Nishiyama S, Garzon A, Parkinson JS. 2014. Mutational analysis of the P1 phosphorylation domain in Escherichia coli CheA, the signaling kinase for chemotaxis. J Bacteriol 196:257-64.

9. Chang AC, Cohen SN. 1978. Construction and characterization of amplifiable multicopy DNA cloning vehicles derived from the P15A cryptic miniplasmid. J Bacteriol 134:1141-56.

10. Yen KM. 1991. Construction of cloning cartridges for development of expression vectors in gram-negative bacteria. J Bacteriol 173:5328-35.

11. Gosink KK, Buron-Barral MC, Parkinson JS. 2006. Signaling interactions between the aerotaxis transducer Aer and heterologous chemoreceptors in Escherichia coli. J Bacteriol 188:3487-93.

12. Amann E, Brosius J, Ptashne M. 1983. Vectors bearing a hybrid trp-lac promoter useful for regulated expression of cloned genes in Escherichia coli. Gene 25:167-78.

13. Sourjik V, Berg HC. 2002. Receptor sensitivity in bacterial chemotaxis. Proc Natl Acad Sci U S A 99:123-7.